72nd International Astronautical Congress (IAC), Dubai, United Arab Emirates, 25-29 October 2021.

IAC-21-D1.IP.3.x66849

Concept of Operations for a Neptune System Mission

James E. McKevitt[a]*, Shayne Beegadhur[a], Louis Ayin-Walsh[a], Franco Criscola[a], Dhrumil Patadia[a], Sophie Bulla[a], Jesus Galinzoga[a], Ramansh Sharma[a], James Morgan[a], Christina Bornberg[a], Tom Dixon[a], Oisín Moore[a], Aryan Laad[a], Ben Wadsworth[a], Kuren M. Patel[a], Jonathan Parkinson-Swift[a], Ethan James[a], Jack Kent[a], Alisa Zaripova[a], Sejal Jain[a], Subin Saji[a], Sreehari Krishnakumar[a], Utkarsh Raj[a]

[a] *Conceptual Exploration Research (Conex),* hello@conexresearch.com
* Corresponding Author

Abstract

The Arcanum mission is a proposed L-class mother-daughter spacecraft configuration for the Neptunian system, the mass and volume of which have been maximised to highlight the wide-ranging science the next generation of launch vehicles will enable. The spacecraft is designed to address a long-neglected but high-value region of the Solar System, showing that current advances make such a mission more feasible than ever before. This paper adds to a series on Arcanum and specifically provides progress on the study of areas identified as critical weaknesses by the 2013 – 2022 Decadal Survey and areas relevant to the recently published Voyage 2050 recommendations to ESA.
Keywords: Neptune, Triton, Astrodynamics, SPH, Telescope, Starship

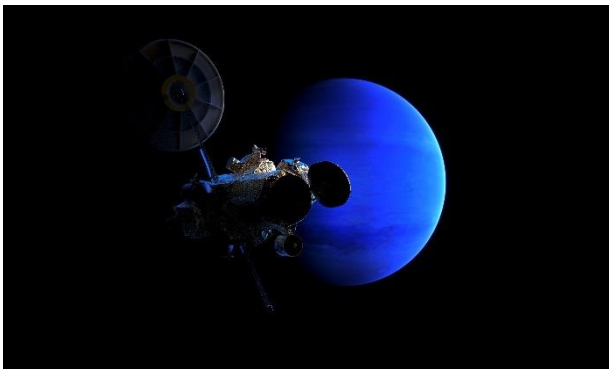

Fig. 1. The Arcanum mission in orbit around Neptune.

1. Introduction

Proposals for missions to the outer Solar System are plentiful and detailed, with a strong science case for a return to this region. Receiving particular focus and as yet remaining without a confirmed mission, the ice giants of Uranus and Neptune present intriguing targets for future Solar System exploration. Indeed, only being visited once by the Voyager 2 spacecraft in the 1980s, advances in planetary science instrumentation routinely deployed elsewhere in the Solar System become clear in comparison and only serve to make a return to these planetary systems more tantalising. Reviews of the future mission landscape from the United States, in the form of the last Planetary Science Decadal Survey (2013 – 2022), stated that a Neptune System orbiter and probe would be of high scientific interest but labelled such an endeavour a 'deferred high-priority mission' given further attention to astrodynamics, delivery cost, suitable power and propulsion, communications, thermal protection and aerocapture were needed. Furthermore, a flyby is advised against given the small cost-saving relative to the decreased science return.

More recently, the Voyage 2050 recommendations to ESA on the European side suggested a future L-class mission is allocated to the exploration of the moons of the giant planets, these including Uranus and Neptune. Noted is the agency's heritage with the success of the Cassini-Huygens mission, which undertook such a task with the Saturnian System, and the soon to fly JUICE, which will explore the moons of Jupiter. A possible dual-spacecraft in a mother-daughter configuration with an additional in-situ element to characterise surface and sub-surface environments is suggested.

The Arcanum mission, consisting of such a spacecraft, is currently under study by Conex Research [1,2] and is designed for operation in the Neptunian system. Aiming to address some areas of concern noted in the Decadal Survey and in light of these new recommendations to ESA, this paper focuses on advances in the study of potential transfers to Neptune and a detailed description of the updated Triton landing system, particularly the addition of a new manoeuvring unit, Tenzing. The spacecraft configuration for the mission can be seen in Fig. 2 and, simply, consists of the primary Neptune orbiter Somerville and the Tenzing Orbital Manoeuvring Unit. Mated to the latter for subsequent detachment once in orbit around Triton are the Bingham soft lander and three surface impact penetrators.

This study takes into consideration the new upper mass limit which can be expected with the next generation of launch vehicle and aims to highlight the advantages to space science these advances will deliver. Further constraint of this design envelope is also detailed in this paper.

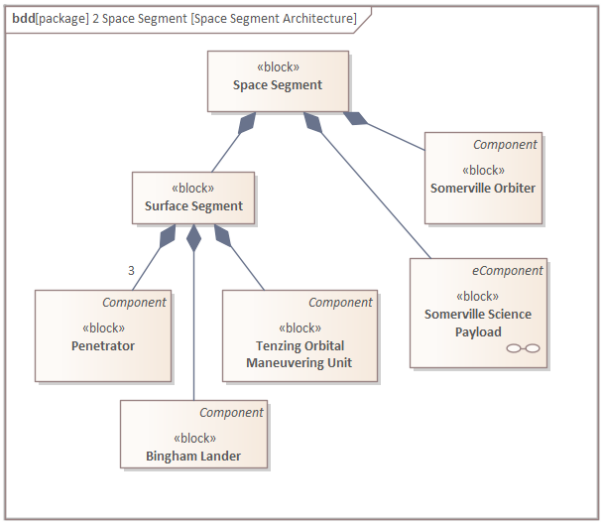

Fig. 2. Configuration of the Arcanum space segment.

The science goals which have guided the finer points of this mission can be found in previous publications of this work [1,2].

2. Launch and mass constraints

When considering the timescales referenced in this proposal, a certain degree of extrapolation is needed to understand the top end lifting capabilities missions will benefit from in the coming decades. Such analysis of the soon-to-be operational super heavy-lift launch vehicles has been carried out in this study and detailed in previous publications [1,2]. However, simply understanding the launchers available is not sufficient. On-orbit and perhaps even cislunar refuelling, 'tugging' and servicing infrastructure can be expected to further raise the upper-level surface to GTO payload mass, and references to such infrastructure by companies such as SpaceX and accompanying funding by NASA are encouraging signs this could be relied upon in the future [3]. In fact, the current NASA-funded Artemis concept of operations includes a number of such refuelling missions [4].

Considering on-orbit infrastructure, a reliable reference point with significant documentation can be taken to be the Lunar Gateway [5]. A refuelling module launching in 2027, specifically the 'European System Providing Refueling, Infrastructure and Telecommunications' (ESPRIT) has been approved and a contractor appointed, limited for the moment to ion engine support. While this will enable planned dynamic lunar operations, it does not yet promise to provide the support to make the Gateway a staging post for deep-space missions, an underpinning feature of the station during its proposal.

Contemplating instead refuelling operations supported from Earth, NASA-funded studies undertaken by SpaceX [3] will ensure the planned Starship-Starship refuels can take place, calculated to increase the vehicle's mass to GTO to 100 tonnes. This is a great increase on the single-launch 21 tonnes to GTO [6].

The Arcanum mission, while designed to highlight the science potential of these increased launch masses, has sought not to under-constrain itself in this area. To this end, a spacecraft mass to GTO possible with one launch has been the goal, with possible expansion to a launch and single refuel.

In attempts to mitigate against an over-weight payload, a number of solutions were investigated:

- Altering the propulsion system or propellant combination in the Earth-departure stage [1].
- Aerobraking at Neptune to reduce the fuel mass needed for capture.
- Launching the Earth-departure stage separately and docking in orbit.

However, it was determined that a single refuel was both sufficient and favourable given the low cost, low operational risk and simplicity of implementation. This ease of expansion of Starship's payload capacity is a perfect demonstration of the significance of its introduction to the launcher market.

3. Transfer to Neptune

3.1 Radiation implications

The spacecraft will experience a number of radiation challenges in deep space, shielding against which provides targeted coverage of sensitive instruments and components. The particularly intense environment around Jupiter, being the strongest experienced during the mission, acts as a design point for the mitigating multi-layer insulating materials of aluminised Mylar, Kapton, Dacron mesh and indium tin oxide.

3.2 Astrodynamics

Designing a deep space trajectory requires the consideration of a number of key points, these being: fuel required, burn efficiency, transfer time and dry mass. These can be managed with a trajectory optimised specifically for this mission, determined in this case using pykep, an ESA-developed astrodynamics tool.

To reduce the transfer delta-V the maximum transfer time, usually inversely proportional to delta-V, was extended to 15 years. Furthermore, a number of gravitational assist manoeuvres were been analysed.

Most gravity assists, or flybys, utilise Jupiter's massive gravitational field to increase the spacecraft's heliocentric velocity. Several examples include Voyagers 1 and 2, Cassini-Huygens and New Horizons [7–9]. In the case of Arcanum, encounters with Venus (V), Earth (E) and Jupiter (J) were identified, combining to form an EVEEJN trajectory. Whilst this clearly increases the mission complexity, the delta-V reduction is seen as justifiable, particularly when considering savings are scaled to the large mass of this mission.

From a geostationary transfer orbit (GTO) at 300 km

Planet	Date	Delta-V (m/s)
Earth (departure)	31st October 2030	3723
Venus	27th June 2031	0.5033
Earth	24th August 2031	0.2146
Earth	11th April 2031	2006
Jupiter	23rd June 2034	0.7332
Neptune (arrival)	30th October 2045	2763
Totals	**15.007 years**	**8403**

Table 1. Trajectory information.

perigee altitude, the spacecraft will increase its total velocity by 3.723 km/s on October 28th, 2030, towards Venus. On June 26th, 2031, the spacecraft will reach closest approach to Venus and perform another burn to increase the velocity by 50.3 cm/s. Somerville will make two flybys of Earth within the next two years, on August 23rd, 2031 and April 10th, 2033, applying two necessary thruster burns of 21.5 cm/s and 2.005 km/s respectively.

On June 23rd, 2034, the spacecraft will perform a 73.3 cm/s burn during closest approach with Jupiter. This will set the spacecraft on a path to Neptune for an expected arrival date on October 27th, 2045. To get into the desired 35000 km by 355000 km orbit, the thrusters finally need to provide a 2.763 km/s capture burn.

In summary, the spacecraft will perform four flybys, bringing the total flight time to approximately 15 years and needing a total delta-V of 8.403 km/s. Illustrations of the planned orbits can be seen in Fig. 3 and Fig. 4.

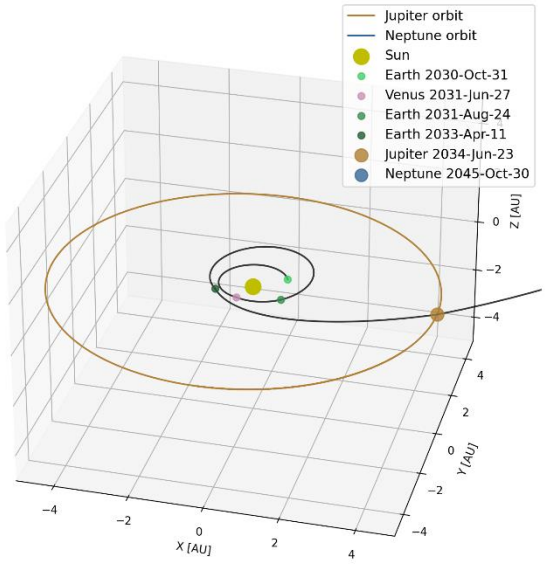

Fig. 3. Superposition of inner planets.

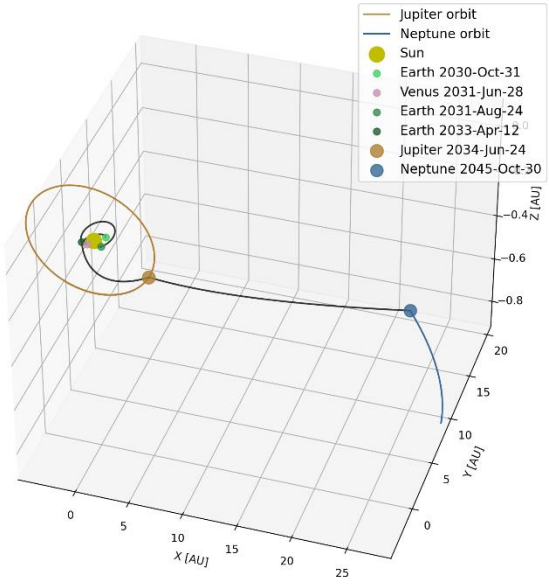

Fig. 4. Jupiter flyby and Neptune arrival.

4. The Triton Vehicles

A principal scientific interest of the mission is the Triton surface and subsurface environment. Access to these is facilitated through three modules: two penetrators, and the soft-landing Bingham probe (Fig. 6 and Fig. 7). These, coupled with the Tenzing Triton-orbit manoeuvring unit, will launch and transit to Neptune together, with Somerville providing power, thermal and communications support for the lander on the journey. Once placed in a highly-eccentric Neptunian orbit, the mated Triton vehicles will be released onto an intercept trajectory with Triton. This course will be set by the orbiter, minimising the fuel expenditure of the Triton vehicles subsystem and therefore maximising propellant available for the landing. This aims to maximise the carrying capacity for scientific instruments capable of operating on the lander, and therefore the science return.

4.1 System Overview

The nexus of the Triton vehicles is the Bingham lander. Once separated from Somerville, it will provide telemetry and power to Tenzing. Bingham will be mounted below Tenzing, while the penetrators will be mounted radially. At the time of deployment, the Triton vehicles will have a total wet mass of approximately 550kg.

4.2 Tenzing Orbital Manoeuvring Unit

4.2.1 Design Overview

The Tenzing Orbital Manoeuvring Unit is introduced to supply the fuel necessary for Triton capture, as well as to fine-tune the Triton orbit and facilitate precise landing site identification while minimising the mass of the final Bingham module itself. Tenzing will have two operating phases: the first, following separation from Somerville and before the separation of Bingham, will involve Tenzing functioning as an integrated service stage, demonstrating minimal autonomy. The second phase, following Bingham separation, will involve Tenzing functioning semi-autonomously. It will run on battery power and have basic orientation control and communications systems to coordinate the time and vector of deployment of the two penetrators.

4.2.2 Integrated Systems

Where Tenzing differs from both a standard tug and part of a multi-stage lander is the degree of integration it has with Bingham, combined with the level of autonomy it maintains when separated. To improve mass efficiency, Bingham and Tenzing will have a single integrated propulsion system: Bingham's primary rocket motors will be configured to drain fuel from Tenzing while the two modules are attached. The two will also feature integrated electronics, with Bingham providing power for Tenzing's essential systems and Tenzing's batteries taking over after separation. Unlike a tug, Tenzing is optimized to conduct the autonomous part of its mission with minimal complexity, thus simplifying the development process.

4.3 Bingham Lander

4.3.1 Design Overview

The Bingham lander's objective is to provide a platform for the study of Triton's atmospheric, surface and subsurface composition. To complete these objectives the lander must carry out a precise soft-landing in Triton's western hemisphere, in the region characterised by 'cantaloupe terrain.' This area is thought to be the oldest portion of Triton's crust and is pockmarked by geysers. Bingham's instrument suite will study the composition of these geysers as well as the ambient atmosphere. Bingham will also be a part of a planet-wide seismic experiment to study the internal dynamics of Triton by measuring the effect of the subsequent penetrator impacts and analysing residual and nominal seismic activity.

4.3.2 Payload

- Cameras
- Seismometer
- Thermometer
- Aerosol Collector and Mass Spectrometer

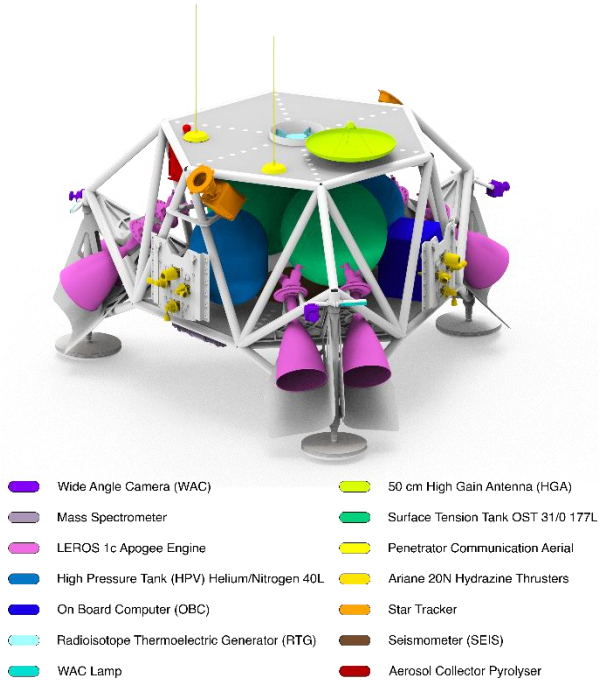

Fig. 5. Colour coded diagram of the Bingham lander.

4.3.3 Structure

The primary structure of Bingham is Ti-6Al-4V titanium-alloy spaceframe consisting of two hexagonal frames 60 degrees out of phase connected by crossbraces. The chosen alloy has a thermal conductivity of 6.7 W/mK [10] reducing the thermal losses from Bingham's structure once in contact with Triton's surface. This primary structure combines the main spacecraft bus, engine mounts and landing legs, reducing downstream integration issues between these subsystems. An interesting feature of the vehicle is the location of the six Leros 1C bipropellant engines being mounted to the primary structure. These engines are fixed at 30 degrees to the vertical inside the structure of the landing legs. This is an example where integrating assemblies in heritage designs into one structure reduces total mass. Additionally, this is a low-mass solution to reduce contamination of the surface by the engine exhaust on descent. This echoes the design of NASA JPL's Skycrane used to land both the Curiosity and Perseverance rovers. Other efforts to reduce mass include using carbon-skin and aluminium hexagonal mesh core sandwich panels for the secondary structures and excluding complex active or passive mechanisms where possible.

A comparable structure would be that of Triton Hopper, where its structural mass is approximately 15 percent of the total mass [10]. A preliminary analysis of Bingham's structure shows that it would weigh just over 10 percent of the total mass. This allows for a greater percentage of mass to be dedicated to the propulsion system which extends the landing range of the vehicle.

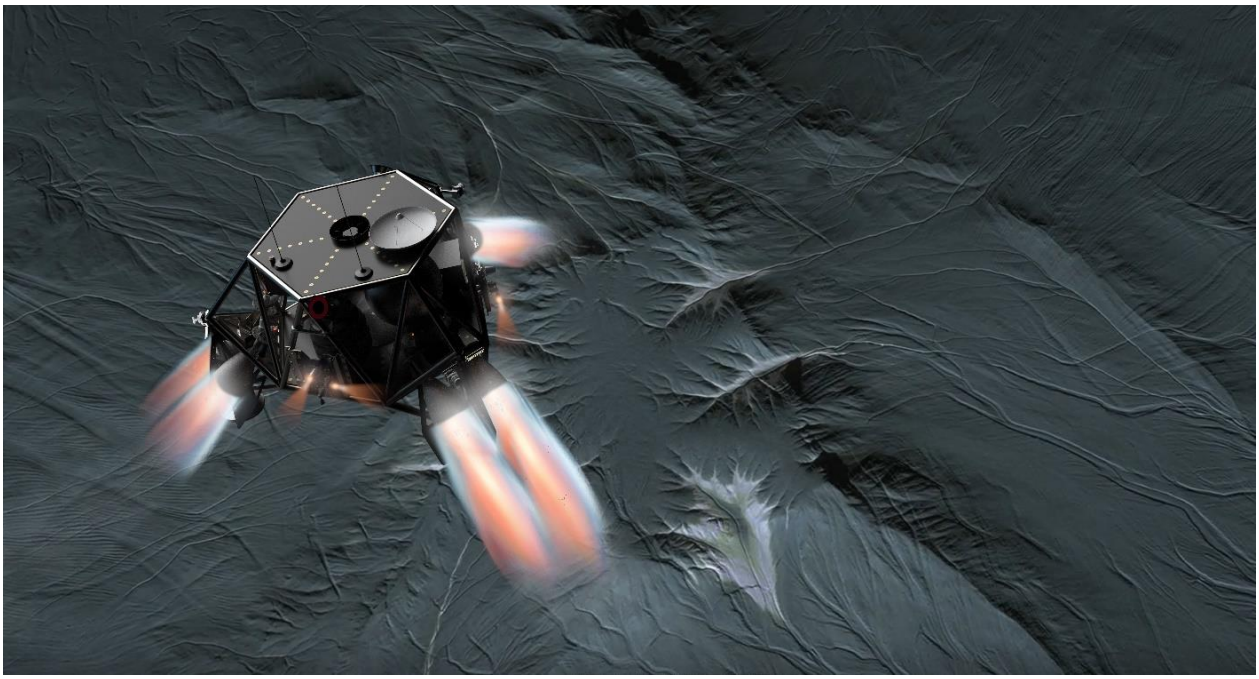

Fig. 6. Render of the Bingham lander on descent to Triton's surface.

This design philosophy will be continued as further analysis of the landing trajectories allows for the structure to be optimised.

Airbags were considered as a means of mitigating the forces experienced during landing on the spacecraft. They can allow reduced fuel loads and can make the spacecraft more durable when it comes to terrain conditions and orientation at impact. An issue that must be addressed is the effect of thruster plumes on the chemical structure of the landing site: there are concerns that this would invalidate some localised experiments. There is also the risk that melting of the local regolith, which is mostly comprised of frozen nitrogen and water, due to engine plumes could cause the lander to become unstable [11], something exacerbated if the landing site is already structurally weak. An airbag system would offer a solution to these difficulties. Heritage airbag landing systems include early Soviet Lunar landers [12], where airbags were used after landing to surround and cushion an ejected payload module and more recently the NASA Mars Exploration Rover Mission operated a more advanced system of lobed Vectran airbags arranged in a tetrahedral structure around the rover [13]. Also considered for this mission were airbags used purely to absorb impact shock of an already-righted spacecraft, in the same manner as the Boeing Starliner. Whilst airbags do help solve the problems of chemical contamination of the landing site, they lack the precision landing ability of engines, and are still dependent on a partially powered descent to ensure the spacecraft is travelling at acceptable speeds at impact, given that any form of aerodynamic deceleration is impossible. The airbags must also deploy rapidly through the use of heavy gas generators and allow the spacecraft to right itself if it lands in an incorrect orientation, then retract to leave the lander set on a rigid structure, something essential for operation of the seismometers.

Opting for a full powered descent aided by rigid landing legs proved to be less operationally complex. The thrusters will be deactivated at an altitude that would cause minimal surface contamination or melting, and crushpads would absorb the remaining impact shock whilst the rigid leg design would minimise structural complexity. Heritage landing leg designs involve telescoping legs with aluminium honeycomb crush core inserts and partially deformable domed footpads. The honeycomb inserts deform to absorb impact energy and an insert in the primary strut is more efficient as all forces are applied along the crushpad's main axis, which is beneficial as lateral compression drastically reduces the material's absorption efficiency. Telescopic legs are responsive to uneven ground conditions, improving the versatility of the lander, and the domed footpads exhibit greater strength than a flat pad of the same mass and can deform in response to uneven regolith, such as in the presence of rocks.

Regardless of this heritage design, the choice of rigid landing legs with crushpads reduces structural mass and complexity. This is the result of the legs being integrated into the primary structure of the spacecraft. Therefore using this type of landing leg, along with the need to have a propulsion system regardless of whether or not airbags are used, is preferred [14].

4.3.4 Propulsion

Of all the locations in which a soft landing has been attempted, Earth's Moon is most similar to Triton (not when it comes to composition and the ambient temperature, but these two factors are still important for longer-term operations). For the landing, two other factors are key: the lack of an atmosphere and the gravity. Mars is dissimilar to Triton due to its atmosphere, with an average surface pressure of 0.636kPa which while thin is not thin enough to be comparable with Triton's atmosphere, which is around 385 times less dense on average. Mars also possesses much higher surface gravity at 3.72m/s^2. Asteroids on the other hand, while also devoid of an atmosphere, have almost no gravity at all. For this reason, this study looked at the landing methods of lunar probes. The most common choice is propulsive landing via rockets. Most descent vehicles, from the Viking landers to the Skycranes of Curiosity and Perseverance, have used storable bipropellant hydrazine engines, with the exception of Starship and Blue Moon. These two, still conceptual, landers use cryogenic propellant. With the desire to maximise the lander mass available for instruments whilst minimising the total wet mass, a staged combustion engine cycle or similar would not be suitable. Looking to minimise complexity and simplify the construction of the spacecraft, while also limiting the potential for mechanical failure to arise during the coast phase of the mission, a pressure-fed or expander cycle system would appear most attractive. The expander cycle offers a high potential specific impulse but is hampered by the need for cryogenic fuel, the long-term management of which would add significant operational complexity to the spacecraft: to prevent boil-off, the fuel must be shielded from even minimal temperature fluctuations. To date, even advanced storage concepts would suit mission durations of 60-90 days, which is far too short for this mission and would require substantial mass gains to make it appropriate [15]. As such, a pressure-fed system was selected. This offers a relatively high specific impulse and a comparatively low associated 'cost' in dry mass due to the lack of required plumbing and turbopumps. The need to optimise propellant pressure against added fuel tank mass means there are practical limits on the combustion chamber pressure. However, the low gravity of Triton means this is acceptable as the minimum required thrust for safe deceleration remains low.

The best precedent for unmanned interplanetary landers to date utilise hydrazine-fuelled engines. The wealth of operational time and experience (TRL 9) of similar systems makes them an attractive choice. Hydrazine and its derivatives can be utilised in both monopropellant and bipropellant systems. The monopropellant option has more precedent when it comes to landers such as Phoenix and Schiaparelli EDM, as well as the Curiosity and Perseverance Skycranes (all designed for use on Mars), simplifying the ignition process and reducing the likelihood of a hard start, something which would be mission-fatal. However when compared against our specific parameters, monopropellant engines prove too inefficient to conduct the full descent burn. Bipropellant options offer a solution to this problem, whilst minimising the increase in hardware complexity. Heritage missions using this technology also align more closely to this mission in that many of them, namely Beresheet and Surveyors 1-7, aimed to make soft landings on the surface of the Moon.

Fuel combinations considered are NTO-MMH, hydrazine-NTO and hydrazine-MON. Other alternative fuels are under consideration in the event that ESA moves to limit the use of hydrazine and other hazardous fuels. A strong cleaner alternative with similar (if not

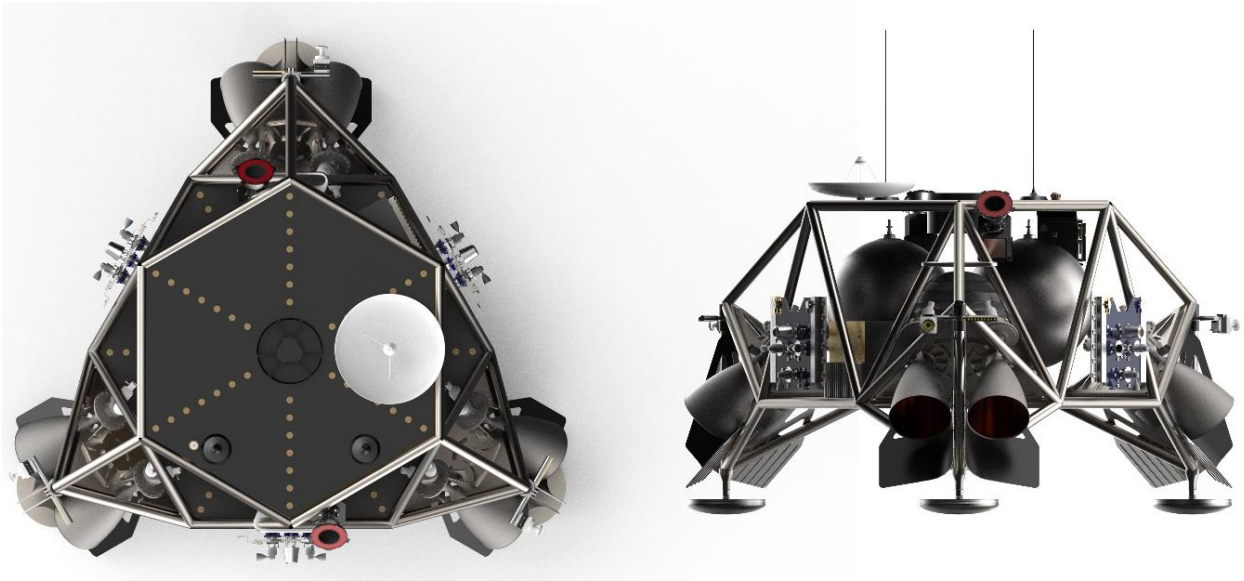

Fig. 7. Render of the Bingham lander.

Subsystems	Launch	Cruise	Separation	Descent	Science	Low Power
Instruments	0	1	0	0	95.3	0
Propulsion	0	0	302	302	0	0
Communications	0	5	24	0	24	5
Thermal Control	0.88	11.88	11.88	11.88	0.88	0.88
Computation/Data	18.5	18.5	22.5	22.5	18.5	14.5
Attitude Control	0	0	94.3	94.3	0	0
Peak Power Draw [W]	19.38	36.38	454.68	430.68	138.68	20.38

Table 2. Bingham Power Breakdown.

improved) propulsive properties would be hydroxylammonium nitrate [16].

With a view to minimising mission costs, commercial off the shelf components are again considered. Fortunately, the experience of European partners in delivering spacecraft propulsion systems for a number of applications means all of Bingham's propulsion hardware is available off the shelf. Primary propulsion is provided by six Nammo Leros 1C Apogee rocket motors [17]. Reaction control thrusters will be Ariane Group 20N Chemical Monopropellant Thrusters [18]. Hydrazine is stored in two Ariane Group Surface Tension tanks, and Helium pressurant will be stored in two MT Aerospace High Pressure tanks.

4.3.5 Power

Given that Bingham's main theatre of operation will, like Somerville's, be the outer Solar System, solar arrays would be an insufficient power system. Battery power alone would be insufficient for the mission's duration but RTG's provide a high-output long-term source of power. However, Plutonium-238 reserves for RTGs are dwindling, driving up production costs and duration. A promising alternative investigated for this mission is Americium-241. Americium RTGs are already being investigated extensively in Europe and have many promising characteristics in terms of availability and lack of required processing: Am-241 is readily available in Europe from nuclear reactor waste processing, and at a much higher level of isotopic purity than Pu-238, manufactured by Neptunium-irradiation. Although the specific power of Am-241 is substantially lower than Pu-238 (114.7 mW/g for Am-241 vs. 390 mW/g for Pu-238), its longer half-life (432.2 years vs. 87 years) means it will supply power more consistently for the duration of the mission [19]. On this mission, a generator will supply 125W of constant power at Triton, used to power essential systems and recharge batteries.

Supplementary power will be supplied by 7.6kg of Eaglepicher Technologies' Lithiated Nickel Cobalt Aluminum Oxide rechargeable batteries, holding over 1070Wh of energy. These are chosen for their impressive spaceflight heritage, including Space Shuttle and Mars missions, and their favourable properties such as long life and good temperature tolerance. The batteries will be drawn upon during the most energy-intensive mission phases such as Triton orbit insertion and landing, supplying up to 500W of power. A breakdown of power production and consumption across the six planned phases of Bingham's mission is given in Table 2.

4.3.6 Avionics

As Bingham will be so far from the Sun, conventional Sun-sensitive orientation control would be ineffective. As such, implemented instead is a novel Triton horizon sensor system combined with conventional star trackers for orientation control. With communications lag times of approximately eight hours between Triton and Earth, the Bingham spacecraft will have to autonomously execute its descent and landing manoeuvres. Once terminal descent begins, Bingham will utilise terrain-relative navigation (TRN) to precisely select a landing site within the pre-determined landing zone. This system will utilise the vehicle's RCS and primary motors, hovering if necessary, to avoid excessively uneven terrain, high gradients or other formations that could damage the vehicle. This system relies on input from optical cameras and Lidar data to generate an accurate map of the local area on the fly, as well as determine the vehicle's velocity and orientation relative to the surface.

Bingham has been designed for a 1.1km/s descent manoeuvre from orbit based on optimising the mass for the current trajectory. This will be refined as the trajectory matures in the design phase and descent will be optimised using TRN to improve the landing performance.

5 Triton Operations

5.1 Selecting Landing Sites

Approximately 40% of Triton's surface was imaged by Voyager 2 (closest approach to Neptune: August 25, 1989, Triton's South Pole was facing the Sun) at sufficient resolution to understand the terrain types [20]. However, this data is both out-of-date and incomplete, requiring further mapping of Triton before landing site selection.

Selecting landing sites is a time-consuming task, sometimes taking more than 4 years [21] due to engineering and scientific requirements [22]. Existing data and that acquired during the transfer to Neptune can

be used for preliminary decision making, whilst higher-resolution data acquired during the Triton orbital phase can be used to refine any decisions. Potential landing sites have been discussed in previous work [1] and include areas characterised by geysers, which are known to move position over time, 'Cantaloupe Terrain' in the western hemisphere and a latitude near the subsolar point for the exploration of cryovolcanism.

5.1.1 Mapping Triton

Constantly improving telescopes, particularly the upcoming JWST, have the potential to provide new data before the arrival of Arcanum to Triton, with the JWST Science Working Group specifically mentioning the trans-Neptunian region as one of interest [23–26]. The telescope component of Somerville could also potentially be used to perform relevant observations during flight for preliminary terrain analysis.

In addition, orbiting of Triton by Tenzing will give mission planners more accurate data than that which currently exists. Therefore, a camera on Bingham for this orbital phase facing Triton is required. This will also help combat the problem of Triton's changing surface, allowing up-to-date and high cadence mapping of the surface both for science and landing purposes.

5.1.2 Expected Surfaces Changes

Triton has complex seasons due to Neptune's axial tilt and the moon's inclined orbit [20,27], therefore changes of the surface and activity are expected.

Table 3. Seasons on Triton [27]. Warm and cold are relative, and may only reflect an absolute temperature change of around 2K

Year	Season
1820	Mild southern summer
1860	Equinox
1910	Cold southern winter
1950	Equinox
2000	Warm southern summer
2040	Equinox
2090	Cold southern winter

Triton has large seasonal variations in its atmosphere. In 1983, Triton was approaching the 'maximum southern summer' and was expected to have a dramatic increase in CH4 abundance within the century [28]. A short summary of Triton's changing environment can be found in Table 3.

5.1.3 Autonomy in Landing Site Selection

Mission planners should be involved in the landing site decision-making process, using the newly gathered data. However, existing concepts of automation can be used to assist their work. A priority concept similar to that used on the Europa Clipper [29] would parse through images of Triton and send back to Earth only the ones that are relevant in the next step of manual analysis, enabling much faster detection of key features such as geysers. Maps including different engineering cartographic data, 'geographical information system (GIS) maps', can be generated and used for representation and evaluation of constraints to find safe landing spots that fulfil scientific and engineering requirements [22].

To further assist planners, machine learning (Bayesian networks, reinforcement learning, transfer learning), can be used for finding potentially suitable landing sites. Bayesian Networks can represent the causal relationships between landing site variables (terrain safety, fuel consumption, and scientific interest). The posterior probability of the model provides the certainty of a terrain region being safe for landing [30]. Reinforcement learning, in combination with transfer learning, can be used for autonomous landing in unknown or barely-known extra-terrestrial environments. Relevant physical phenomena learned by 3D mesh data from NASA can be used as a base for simulating Triton's surface by using transfer learning with newly obtained data [31].

5.2 Ionosphere reflection experiment

Radio waves of different frequencies are a useful tool for remote sensing and measurement. A well-established technique, this has been successfully used onboard spacecraft such as Cassini [32] and New Horizons [33] and in the case of Arcanum, offers an interesting repurposing of already-essential communications equipment. For this use case, three different radio experiment setups have been identified:

1) Radio occultation between Earth and Somerville.
2) Radio occultation between Bingham and Somerville.
3) Ionosphere radio bounce off between the penetrators and Bingham.

Results from the Voyager 2 radio occultation experiment showed an unexpectedly strong ionosphere around Triton, with a single layer beginning at about 200 km and peaking at about 350 km. The peak electron density measured was about $23 \times 10^9\ m^{-3}$ at ingress and $46 \times 10^9 m^{-3}$ at egress [34], the difference being down to the ingress location not being subjected to any sunlight during the previous Triton day. It is currently unknown how much ionisation is caused by the Sun and how much by interaction with Neptune. 1989, the date of the flyby, was during the solar maximum of solar cycle 22, the fourth strongest solar cycle on record [34]. As the arrival of the Arcanum probes on Triton may occur during solar minimum or a much weaker solar maximum, it is important to consider how the intensity may be decreased. Assuming the peak density decreases by half at solar minimum, this gives a lower peak density value

of about $13 \times 10^9\ \mathrm{m}^{-3}$ during a day that receives no sunlight. However, further research must be completed to reach a more accurate picture of the expected density.

One experiment performed by the Arcanum mission will measure the long-term changes of density at different heights in Triton's ionosphere. To do this, the impact penetrators will emit radio pulses in the MF-band which bounce off of the ionosphere and are detected by Bingham. These pulse emissions of defined frequency and strength are timed by chronometers so that Bingham can determine the runtime and attenuation. The distance between the penetrators and Bingham must be known precisely and be low enough so that the radio pulse can reach Bingham in one reflection of the ionosphere.

Whilst the surface of Triton is relatively smooth, larger terrain features may still interfere with the beam at large launch angles. At a launch angle of 90°, the beam will travel very closely to the surface for at least a few kilometres. It is therefore advisable to have an approximate maximum launch angle of 80°. At this angle, the radius of Triton (1350 km) and height of the layer (reflection will occur between 200 km and 350 km) give a furthest distance of about 1120 km between landing sites for a 1 hop transmission.

6 Penetrators and Seismology

As previously stated, Arcanum consists of the Somerville orbiter, Tenzing manoeuvring unit, Bingham landing probe and Triton penetrators, the latter of which will be the focus of discussion within this section, detailing the initial investigation into the penetrator nose design as part of this design iteration.

The investigation evaluated penetrator nose designs with a tangent ogive profile and varying calibre radius head (CRH) values, further introduced in the following section, to determine the optimum nose profile for maximum surface penetration, thereby reducing the required impact velocity and subsequently the impact forces occurring on the penetrator structure during surface contact.

6.1 Theoretical Penetration Depth

Due to Triton's surface being comprised predominantly of frozen nitrogen, water, and carbon dioxide, theoretical penetration depths (D) were calculated using Young's penetration equation for Ice and solids, shown in equation (1) [35]. The definition of each variable and their corresponding units for this equation and each subsequent equation within this section are displayed in Table 4.

$$D = 4.6 \times 10^{6}\ \mathrm{S}\ \mathrm{N}\ \left(\frac{\mathrm{m}}{\mathrm{A}}\right)^{0.6}\ (\mathrm{V} - 30.5)\ \ln(50 + 0.29\mathrm{m}^2) \quad (1)$$

Young's equation utilises both the penetrator's nose performance coefficient and the surface's penetrability (S – number) which are denoted as *N* and *S* respectively. The former of these was determined using equation (2) applicable for any given tangent ogive nose profile. A representation of this nose profile, detailing its dimensions with corresponding variables, is presented in Fig. 8 below.

$$\mathrm{N} = 0.18\left(\frac{\mathrm{L_n}}{\mathrm{d_p}}\right) + 0.56 \quad (2)$$

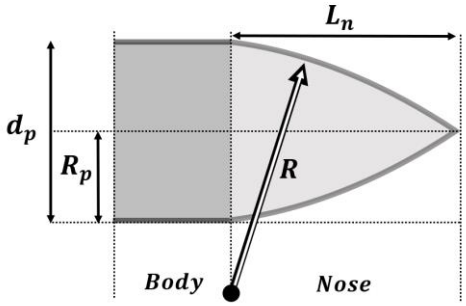

Fig. 8. Tangent ogive nose profile dimensions.

For ice exceeding a depth of 10 ft (3.048 m), a typical S-number is estimated to be approximately between 1 and 2 [36]. Therefore a value of 1.5 was selected for the initial penetration depth calculations.

As previously stated, this investigation evaluated varying nose CRH values. Therefore, the penetrator nose length $\mathrm{L_n}$ utilised within equation (2) can subsequently be determined using equation (3) with respect to a given CRH value.

$$\mathrm{L_n} = \sqrt{\left(\mathrm{d_p} \cdot \mathrm{R}\right) - \left(\mathrm{R_p}\right)^2} \quad (3)$$

The resulting theoretical penetration depths calculated from these aforementioned equations was subsequently used to validate simulated data, the results of which will be introduced and analysed within the following sections.

Table 4. Young's equation variables.

Symbol	Description	Unit
D	Penetration depth	m
S	Surface penetrability	-
N	Nose performance coefficient	-
m	Penetrator mass	kg
A	Cross-sectional area	m^2
L_n	Penetrator nose length	m
d_p	Penetrator diameter	m
R	Ogive radius	m
R_p	Penetrator radius	m

6.2 Simulation Methodology

This section provides a brief overview into the methodology of the simulations conducted throughout this investigation. These impact simulations between the penetrator lower section and Triton's surface were undertaken using Ansys Explicit Dynamics in conjunction with SolidWorks and Ansys workbench for CAD modelling and mesh generation respectively. A coupled SPH-FEM method was used, with smoothed-particle hydrodynamics (SPH) used to model the dynamic surface of Triton and a finite-element method used to model the rigid penetrator. SPH is both efficient and accurate in high-energy impact simulations such as these, and there is precedence of modelling similar space applications with SPH [37].

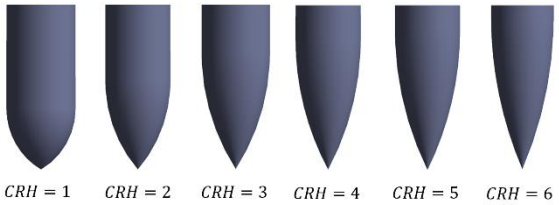

Fig. 9. Simulation penetrator nose profiles.

Fig. 9 illustrates simplified penetrator nose profiles with increasing CRH values from 1 to 6 used within these simulations. Each profile utilised a hybrid mesh of hexahedral and tetrahedral elements with the latter assigned towards the lower nose section. Due to the aim of this investigation solely focusing on the penetration depth within Triton's surface after impact, the penetrator body was assigned a rigid stiffness behaviour thereby preventing deformation.

Triton's surface model was simplified as a cuboid positioned directly below the penetrator model as shown in Fig. 10. Unlike the penetrator, Triton's surface was assigned a flexible stiffness behaviour to enable deformation to occur, thereby enabling the recording of penetration depths for each nose profile to be undertaken during post-processing.

Triton's surface material properties were approximated using the material properties of ice with a density of $\rho = 917\ \mathrm{kg\,m^{-3}}$ and a Young's modulus of $E = 9.1 \times 10^{-9}\ \mathrm{Pa}$. Each penetrator was assigned a preliminary mass of 50 kg and an initial vertical velocity downward component of $200\mathrm{ms}^{-1}$, the values of which were previously used within the theoretical calculations introduced in the previous section, thereby allowing a validation of the simulation results to be undertaken. The results of this, in conjunction with the final theoretical and simulation results of this investigation are presented and discussed within the following section.

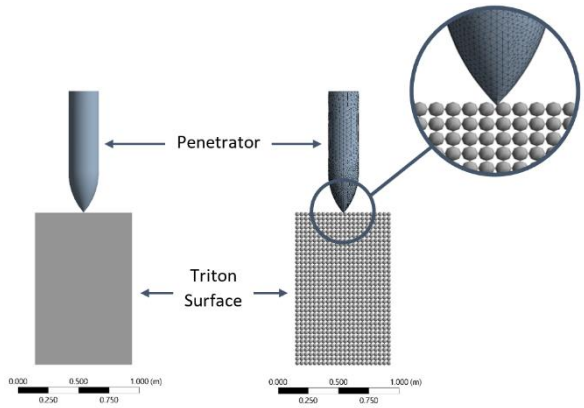

Fig. 10. Simplified penetrator and Triton surface side profile. Model geometry (left), model mesh with close-up (right).

6.3 Penetration Depth Results and Discussion

As previously discussed, a validation and sensitivity study was initially conducted between theoretical calculations using Young's penetration equations and simulation data accrued through the use of Ansys explicit dynamics for a nose profile of CRH = 4. It was observed that an error of approximately 10% between the two results was present after subsequent mesh refinements were undertaken. This was deemed to be an acceptable error, albeit marginally high. Further mesh refinement may lead to a lower discrepancy between the two results. However, due to software license limitations and the resulting increased computational expense from the greater number of elements of generated by such mesh refinements, these were not undertaken, though such investigations may be reserved for future publications. The results of the validation and sensitivity study demonstrated that Young's theoretical results can be successfully reproduced within the selected simulation software. Therefore, further simulations were subsequently conducted for the remaining CRH models previously illustrated in Fig. 9.

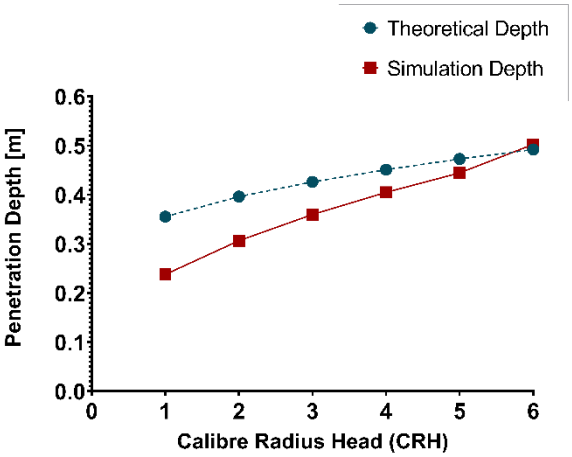

Fig. 11. Penetration depth results of varying CRH.

It was observed that increasing the penetrator's nose CRH value resulted in the increase in its penetration depth after impact, as illustrated by the upwards trend in Fig. 11. A comparison of results between theoretical calculations and simulations shows that as CRH decreases, the error between the two data sets increases and subsequently the reliability of the simulation results decreases. Therefore, future investigations should aim to address this but it can still be clearly seen that both theoretical and simulation results follow a similar trend and therefore confidence in their correlation can be established. Comparing the results of the lowest and highest CRH nose profiles at CRH = 1 and CRH = 6 respectively, it was observed that the difference in penetration depth was approximately 0.2649 m, seen in Fig. 12, representing an increase of 111.4%.

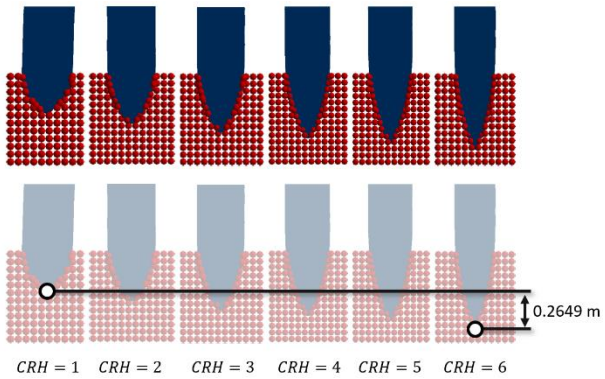

Fig. 12. Graphical results comparing the effects of CRH on penetration depth.

The increase in penetration depth attributed to the increase in CRH value implies that a tangent ogive nose profile with a larger CRH should be considered for use within future penetrator design iterations. This would allow for the penetrator to achieve its desired penetration depth at a lower impact velocity thereby reducing the impact forces incurred on its structure allowing for increased chance of survivability during contact with Triton's surface. Furthermore, this reduced impact force would potentially allow for fewer structural reinforcements to be considered within the penetrator design phase thereby reducing the overall structural mass.

This investigation aimed to provide a basis for the penetrator profile design by proving that an increase in a given nose profile's CRH value would result in increased penetration depth. This was supported by theoretical calculations using Young's penetration equations and replicated within simulation software thereby providing a platform in which higher fidelity simulations can be undertaken thus increasing the accuracy of the results with the final intent of accurately predicting the penetrator's final depth after impact. The process and results of such investigation in conjunction with a structural analysis evaluating the potential of deformation to occur on the projectile during impact shall be reserved for future publications.

5 Telescope

As an integral part of the Somerville Orbiter, a telescope operating within the visible and near-infrared (0.3–1.5μm), and with a 0.7-metre aperture for the primary mirror, is proposed. An instrument with such capabilities, operating in the outer Solar System beyond the influence of sunlight scattered by interplanetary dust, 'zodiacal light', is regarded as a powerful tool in answering a large number of science goals [38].

Other space-based observatories were used as a reference to define the design requirements for the Somerville telescope. A science-driven design method, such as has previously been proposed [39] considering the observation of KBOs and Planet-Nine-like objects whilst orbiting Neptune was used to define the requirements of the optical system.

A standard configuration two-mirror Cassegrain reflector was proposed as a starting point in order to define the focal length and overall dimensions. However, a Ritchey-Cherétien (RC) scheme with a concave hyperbolic primary mirror is regarded as a more capable alternative as such arrangement reduces coma and spherical aberration.

To begin the design process, a calculated focal length is inserted into established relationships for an optimally constructed optoelectronic telescope system [40].

$$f = \frac{\mathrm{D}\,\rho_{\mathrm{lim}}\mathrm{l}_{ps}}{\lambda_p} \tag{4}$$

where D is the aperture diameter, ρ_{lim} is the coefficient for resolution limit defined by the Rayleigh Criterion as 0.8086 ± 0.08, $\mathrm{l_{ps}}$ is the size of each photodetector element and λ_{p} is the average value of the selected wavelength range. After this, the following geometrical parameters for the RC scheme were calculated directly, resulting in the specifications shown in Table 5.

Table 5. Telescope design specifications.

Parameter	Baseline	Units
Scheme	RC obstructed, on-axis pupil	-
Primary Ø	0.7	m
Primary hole Ø	0.18	m
Photodetector element pixel size	12	μm
Focal length	7.56	m
f-number	f/11	m
Waveband	0.3 - 1.5	μm
Angular resolution	0.1 - 0.54	arcsec

Moreover, a 2D ray-trace simulation of the proposed configuration was performed from which it was possible to define the curvature, sphericity and position of the focal plane (FP), primary mirror (M1) and secondary mirror (M2). The results are shown in Table 6 and Fig. 13.

Table 6. CRC scheme, distribution and dimensions (m).

Element	Position	Curvature	Asphericity	Diameter	Hole diameter
M1	1.97	-0.197	-1.004	0.7	0.18
M2	-	-0.661	-1.602	0.21	-
FP	-2.27	-	-	0.15	-

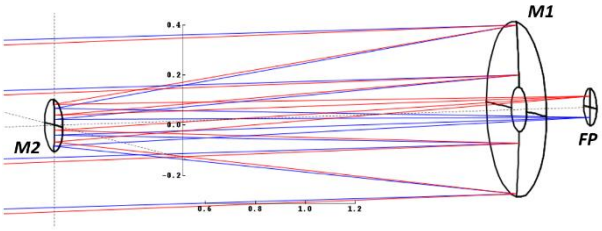

Fig. 13. 2D ray trace for the two-mirror curved RCT.

To determine the mass of the telescope, a previously proposed statistical model [41] is used in order to calculate the approximate total weight of the optical system. Considering the aperture diameter as a defining feature, the model presented in Fig. 14 describes the equivalence in mass for an aperture up to 1.7-meter.

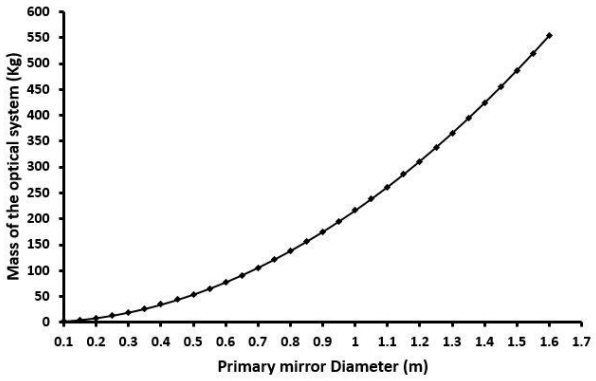

Fig. 14. Mass analysis for a CRC two-mirror telescope.

6 Conclusions

Any space mission design requires a multifaced approach, and Arcanum is no exception. As part of the ever-growing series of papers on this mission, here Conex present their latest development work on the Triton segment of the mission, a suitable transfer trajectory to Neptune and specifications for the Somerville telescope.

Concepts for the next outer Solar System mission have long been proposed, but now the time is approaching where payload masses and cost reductions mean the science performed by such missions justifies the efforts needed to support them. Arcanum represents a successful, data-driven study in the viability of such missions, and should serve as a new reference point for the next round of proposed spacecraft.

Acknowledgements

This work represents a truly international effort, uniting like-minded young researchers from around the world. The self-starting of this group, the complete remote working, and their dedication and perseverance shown in the face of COVID-19 disruption is a testament to each and every character involved in the team.

Partners providing software and technical advice are thanked for their support and their belief in the Conex project – Sydereal, tukom, Sparx Systems, Jundroo and Patchion.

References

[1] J. McKevitt, C. Bornberg, T. Dixon, L. Ayin-Walsh, J. Parkinson-Swift, J. Morgan, S. Beegadhur, F. Criscola, C. Heinreichsberger, B. Simha Reddy Pappula, S. Bulla, K.M. Patel, A. Laad, E. Forder, J. Singh, O. Moor, M. Foghis, P. Wedde, T. McDougall, J. Kent, U. Raj, The Arcanum Mission: Scientific Objectives and Instruments for Neptune, Triton and KBOs, J. Br. Interplanet. Soc. 74 (2021) 26–35.

[2] J. McKevitt, S. Bulla, T. Dixon, F. Criscola, J. Parkinson-Swift, C. Bornberg, J. Singh, K. Patel, A. Laad, E. Forder, L. Ayin-Walsh, S. Beegadhur, P. Wedde, B.S.R. Pappula, T. McDougall, M. Foghis, J. Kent, J. Morgan, U. Raj, C. Heinreichsberger, An L-class Multirole Observatory and Science Platform for Neptune, in: Glob. Sp. Explor. Conf., International Astronautical Federation, St. Petersburg, 2021.

[3] C. Skelly, National Aeronautics and Space Administration, NASA Announces Partners to Advance "Tipping Point" Technologies, Washington DC, 2020.

[4] M. Witt, J. Rowe, National Aeronautics and Space Administration, NASA Picks SpaceX to Land Next Americans on Moon, Washington DC, 2021.

[5] National Aeronautics and Space Administration, FY 2022 Budget Request, Washington DC, 2021.

[6] Space Exploration Technologies Corp. (SpaceX), Starship Users Guide Rev 1.0, 2020.

[7] B.A. Smith, L.A. Soderblom, D. Banfield, C.

Barnet, A.T. Basilevksy, R.F. Beebe, K. Bollinger, J.M. Boyce, A. Brahic, G.A. Briggs, R.H. Brown, C. Chyba, S.A. Collins, T. Colvin, A.F. Cook, D. Crisp, S.K. Croft, D. Cruikshank, J.N. Cuzzi, G.E. Danielson, M.E. Davies, E. De Jong, L. Dones, D. Godfrey, J. Goguen, I. Grenier, V.R. Haemmerle, H. Hammel, C.J. Hansen, C.P. Helfenstein, C. Howell, G.E. Hunt, A.P. Ingersoll, T. V. Johnson, J. Kargel, R. Kirk, D.I. Kuehn, S. Limaye, H. Masursky, A. McEwen, D. Morrison, T. Owen, W. Owen, J.B. Pollack, C.C. Porco, K. Rages, P. Rogers, D. Rudy, C. Sagan, J. Schwartz, E.M. Shoemaker, M. Showalter, B. Sicardy, D. Simonelli, J. Spencer, L.A. Sromovsky, C. Stoker, R.G. Strom, V.E. Suomi, S.P. Synott, R.J. Terrile, P. Thomas, W.R. Thompson, A. Verbiscer, J. Veverka, Voyager 2 at Neptune: Imaging Science Results, Sci. 246 (1989) 1422–1449.

[8] National Aeronautics and Space Administration, CASSINI. Report on the Phase A study: Saturn Orbiter and Titan probe, Washington, DC, United States, 1988.

[9] Y. Guo, R.W. Farquhar, New Horizons Mission Design, Space Sci. Rev. 140 (2007) 49–74.

[10] S.R. Oleson, G. Landis, Triton Hopper: Exploring Neptune's Captured Kuiper Belt Object, in: Planet. Sci. Vis. 2050 Work., NASA Planetary Science Division, Washington DC, 2017.

[11] B.J. Holler, L.A. Young, W.M. Grundy, C.B. Olkin, On the surface composition of Triton's southern latitudes, Icarus. 267 (2016) 255–266.

[12] T. Gold, Probable mode of landing of Luna 9, Nature. 210 (1966) 150–151.

[13] J.A. Crisp, M. Adler, J.R. Matijevic, S.W. Squyres, R.E. Arvidson, D.M. Kass, Mars Exploration Rover mission, J. Geophys. Res. Planets. 108 (2003) 8061.

[14] A. Sahinoz, Landing Gear Design and Stability Evaulation of a Lunar Lander, in: Bennett Conf. Mech. Eng., Pittsburgh, PA, 2012.

[15] M.P. Doherty, M.L. Meyer, S.M. Motil, C.A. Ginty, Cryogenic Propellant Storage and Transfer (CPST) Technology Maturation: Establishing a Foundation for a Technology Demonstration Mission (TDM), in: AIAA Sp. 2013 Conf. Expo., American Institute of Aeronautics and Astronautics, San Diego, CA, 2013.

[16] R.A. Spores, R. Masse, S. Kimbrel, C. McLean, GPIM AF-M315E Propulsion System, in: AIAA/ASME/SAE/ASEE Jt. Propuls. Conf., American Institute of Aeronautics and Astronautics, Cleveland, OH, 2014.

[17] Nammo, LEROS 1c Apogee Engine, Westcott, 2021.

[18] ArianeGroup Orbital Propulsion, 1N, 20N, 400N and Heritage Thruster, Chemical Monopropellant Thruster Family, Taufkirchen, 2021.

[19] R.M. Ambrosi, H. Williams, E.J. Watkinson, A. Barco, R. Mesalam, T. Crawford, C. Bicknell, P. Samara-Ratna, D. Vernon, N. Bannister, D. Ross, J. Sykes, M.C. Perkinson, C. Burgess, C. Stroud, S. Gibson, A. Godfrey, R.G. Slater, M.J. Reece, K. Chen, K. Simpson, R. Tuley, M. Sarsfield, T.P. Tinsley, K. Stephenson, D. Freis, J.F. Vigier, R.J.M. Konings, C. Fongarland, M. Libessart, J. Merrifield, D.P. Kramer, J. Byrne, B. Foxcroft, European Radioisotope Thermoelectric Generators (RTGs) and Radioisotope Heater Units (RHUs) for Space Science and Exploration, Space Sci. Rev. 215 (2019) 1–41.

[20] W.B. McKinnon, R.L. Kirk, Triton, in: T. Spohn, D. Breuer, T. V. Johnson (Eds.), Encycl. Sol. Syst., 3rd ed., Elsevier, 2014: pp. 861–881.

[21] M. Golombek, J. Grant, D. Kipp, A. Vasavada, R. Kirk, R. Fergason, P. Bellutta, F. Calef, K. Larsen, Y. Katayama, A. Huertas, R. Beyer, A. Chen, T. Parker, B. Pollard, S. Lee, Y. Sun, R. Hoover, H. Sladek, J. Grotzinger, R. Welch, E. Noe Dobrea, J. Michalski, M. Watkins, Selection of the Mars Science Laboratory Landing Site, Space Sci. Rev. 170 (2012) 641–737.

[22] M. Pajola, S. Rossato, E. Baratti, A. Kling, Planetary Mapping for Landing Sites Selection: The Mars Case Study, Planet. Cartogr. GIS. (2019) 175–190.

[23] G. Sonneborn, M. Clampin, H. Hammel, JWST Science Working Group, JWST Study of Planetary Systems and Solar System Objects, 2009.

[24] J. Lunine, H. Hammel, E. Schaller, G. Sonneborn, G. Orton, G. Rieke, M. Rieke, JWST Planetary Observations within the Solar System, 2010.

[25] J. Norwood, H. Hammel, S. Milam, J. Stansberry, J. Lunine, N. Chanover, D. Hines, G. Sonneborn, M. Tiscareno, M. Brown, P. Ferruit, Solar System Observations with JWST, 2014.

[26] H.B. Hammel, M. El Moutamid, L. Fletcher, B. Holler, M.S.P. Kelley, H. Melin, S. Milam, C. Nixon, J. Norwood, A. Parker, A. Rivkin, P. Santos-Sanz, G. Sonneborn, J. Stansberry, M. Tiscareno, C. Thomas, G.L. Villanueva, Solar System Science with the James Webb Space Telescope Co-authors: , 2019.

[27] R. Schmude, Uranus, Neptune, and Pluto and How to Observe Them, Springer New York, New York, NY, 2008.

[28] L. Trafton, Large seasonal variations in Triton's atmosphere, Icarus. 58 (1984) 312–324.

[29] K.L. Wagstaff, G. Doran, A. Davies, S. Anwar, S. Chakraborty, M. Cameron, I. Daubar, C. Phillips, Enabling onboard detection of events of scientific interest for the Europa clipper spacecraft, in: Proc. ACM SIGKDD Int. Conf. Knowl. Discov. Data Min., Association for Computing Machinery, 2019: pp. 2191–2201.

[30] N. Serrano, A Bayesian framework for landing site selection during autonomous spacecraft descent, in: IEEE Int. Conf. Intell. Robot. Syst., IEEE, Beijing, 2006: pp. 5112–5117.

[31] G. Ciabatti, S. Daftry, R. Capobianco, Autonomous Planetary Landing via Deep Reinforcement Learning and Transfer Learning, in: 2021 IEEE/CVF Conf. Comput. Vis. Pattern Recognit. Work., IEEE, 2021: pp. 2031–2038.

[32] A.J. Kliore, J.D. Anderson, J.W. Armstrong, S.W. Asmar, C.L. Hamilton, N.J. Rappaport, H.D. Wahlquist, R. Ambrosini, F.M. Flasar, R.G. French, L. Iess, E.A. Marouf, A.F. Nagy, Cassini Radio Science, in: C.T. Russell (Ed.), Cassini-Huygens Mission, Springer, Dordrecht, 2004: pp. 1–70.

[33] G.L. Tyler, I.R. Linscott, M.K. Bird, D.P. Hinson, D.F. Strobel, M. Pätzold, M.E. Summers, K. Sivaramakrishnan, The New Horizons Radio Science Experiment (REX), Space Sci. Rev. 140 (2008) 217–259.

[34] G.L. Tyler, D.N. Sweetnam, J.D. Anderson, S.E. Borutzki, J.K. Campbell, V.R. Eshleman, D.L. Gresh, E.M. Gurrola, D.P. Hinson, N. Kawashima, E.R. Kursinski, G.S. Levy, G.F. Lindal, J.R. Lyons, E.A. Marouf, P.A. Rosen, R.A. Simpson, G.E. Wood, Voyager Radio Science Observations of Neptune and Triton, Science (80-.). 246 (1989) 1466–1473.

[35] C.W. Young, Penetration Equations, Albuquerque, 1997.

[36] R.S. Bernard, Depth and Motion Prediction for Earth Penetrators, Vicksburg, 1978.

[37] P. Weiss, K.L. Yung, N. Kömle, S.M. Ko, E. Kaufmann, G. Kargl, Thermal drill sampling system onboard high-velocity impactors for exploring the subsurface of Europa, in: Adv. Sp. Res., Elsevier Ltd, 2011: pp. 743–754.

[38] J. Bock, C. Beichman, A. Cooray, W. Reach, R.-R. Chary, M. Werner, M. Zemcov, Astronomical opportunities from the outer solar system, SPIE Newsroom. (2012).

[39] H.P. Stahl, G. Kuan, W.R. Arnold, T. Brooks, J.B. Knight, S. Martin, Habitable-Zone Exoplanet Observatory baseline 4-m telescope: systems-engineering design process and predicted structural thermal optical performance, J. Astron. Telesc. Instruments, Syst. 6 (2020) 034004.

[40] V.I. Kurenkov, S.P. Koroleva, Fundamentals of designing spacecraft for optical-electronic observation of the Earth's surface. Calculation of the main characteristics and the formation of the project appearance, Publishing house Samar. un-ta, 2020.

[41] V.I. Malamed, Design of Space Based Optical Devices, St. Petersburg State Instituted of Precise Mechanics and Optics, St. Petersburg, Russia, 2002.